Partial Crystallization of an Amorphous Alloy by Electronic Energy Deposition

A. Dunlop,* G. Jaskierowicz, and G. Rizza
Laboratoire des Solides Irradiés, Commissariat à l'Energie Atomique/Ecole Polytechnique, 91128 Palaiseau, France

M. Kopcewicz
Institute of Electronic Materials Technology, Wolczynska 133, 01-919 Warszawa, Poland
(Received 13 August 2002; published 9 January 2003)

The first experimental evidence is reported of crystallization induced in an amorphous alloy by a high density of electronic excitation deposited along the path of swift heavy ions. The formation of nanocrystalline iron boride phases was observed in an amorphous $Fe_{73.5}Cu_1Nb_3Si_{13.5}B_9$ alloy irradiated at low temperature with 5 GeV Pb ions up to fluences of 1×10^{11} ions cm^{-2}. No evidence for the formation of the Fe(Si) phase was found. This phenomenon was interpreted in terms of the relaxation of the high level of energy deposited in electronic excitations along the path of Pb ions in the target, which induces extensive stress and strain that could destabilize the amorphous structure.

DOI: 10.1103/PhysRevLett.90.015503 PACS numbers: 61.80.Jh, 61.43.Dq, 61.43.Er, 68.37.Lp

Introduction.—The passage of a swift ion through matter mainly leads to the electronic excitation and ionization of target atoms. During this process ($\leq 10^{-17}$ s) showers of excited δ electrons are ejected around the path and a very high space-charge density is created ($\sim 10^{-15}$ s). In metallic systems, the lifetime of a space charge is limited due to the rapid screening by the conduction electrons ($\sim 10^{-13}$ s). The residual damage depends on the nature of the target and on the amount of energy deposited into electronic processes (S_e).

In the early 1980s, for the first time a spectacular macroscopic deformation ($\sim 10\%$) of amorphous targets, named "anisotropic growth," was found [1–4]. This effect, which consists in a shrinking of the sample along the beam direction and an expansion perpendicular to the beam direction, is observed above a threshold in the rate of energy deposition into electronic processes ($S_e^{\text{th}} \sim 10$ keV $\cdot$ nm^{-1}) and above a critical irradiation fluence Φ_c. These observations were interpreted as follows [5,6]: (i) below Φ_c, damage is introduced in the amorphous structure along the path of each projectile, leading to the creation of additional free volume and thus of cylinders of "modified" amorphous matter; (ii) above Φ_c, the anisotropic growth results from radial movements of atoms perpendicular to the ion beam direction, but the structure of the irradiated material remains amorphous. Later on many unexpected irradiation effects induced by S_e were experimentally observed in pure metals, e.g., phase transformation [7], and defects annealing and creation [8,9]. It is now unambiguously established that high electronic excitation can play an important role in damage processes of metallic targets under swift heavy ion irradiation.

Transmission electron microscopy (TEM) observations of the surface deformations on both sample surfaces of these amorphous samples [10,11] permit the determination of the cross sections of the residual cylinders of modified matter.

In this Letter we present the first experimental evidence of a crystallization process induced in an amorphous alloy irradiated at low fluences by GeV monoatomic ions. This crystallization is observed in the vicinity of the cylinders of "modified" amorphous matter. For this study we selected an amorphous $Fe_{73.5}Cu_1Nb_3Si_{13.5}B_9$ alloy which is of interest because it serves as a precursor for the formation of the soft magnetic nanocrystalline phase [12]. As this alloy is characteristic of a particular class of amorphous alloys exhibiting two step crystallization, it is interesting to study the behavior of such an alloy submitted to high electronic energy deposition.

Experimental.—The samples used in this study were amorphous $Fe_{73.5}Cu_1Nb_3Si_{13.5}B_9$ ribbons prepared by the melt spinning technique. It was checked by x-ray diffraction and Mössbauer measurements that the ribbons were fully amorphous. The targets in the form of 3 mm diameter disks were electrochemically prethinned for TEM observations and mounted in a liquid nitrogen cryostat installed on the GANIL accelerator in Caen (France). Irradiations with 5 GeV incident Pb ions were performed at normal incidence under a controlled ion flux ($< 5 \times 10^8$ ions $\cdot$ cm^{-2} $\cdot$ s^{-1}), which limits the sample temperature to stay well below 90 K. Pb ions in the alloy have a rate of energy deposition into electronic processes of $S_e \sim 40$ keV $\cdot$ nm^{-1}. Samples irradiated up to fluences of 1×10^{11} ions $\cdot$ cm^{-2}, slowly warmed to room temperature, were then examined in a 300 kV transmission electron microscope (Philips CM30). Observations were performed using the phase contrast technique, which consists of defocusing the objective lens of the microscope to give rise to a phase contrast (Fresnel fringes) inside the ion deformed regions (tracks). High resolution transmission electron microscopy (HRTEM) micrographs were processed with a slow scan CCD camera and analyzed with the digital micrograph program. The TEM observations were always performed using a very

low electron flux in order to avoid any structural modification of the sample induced by the electron beam.

Results.—The main results deduced from the TEM observations are summarized in Table I. The TEM micrographs and electron diffraction patterns are presented in Fig. 1. Figure 1(a) shows a bright field electron micrograph of an unirradiated sample. As expected, no contrast is visible. The electron diffraction pattern [Fig. 1(c)] is characteristic of an amorphous alloy. It consists of two very wide diffraction rings, hereafter referred to as $A1$ and $A2$. The first one, $A1$, is centered at a position corresponding to an "interplanar distance" $d = 2.033$ Å, which according to the Guinier formula [13] corresponds to an average distance between atoms x_m in the amorphous structure $x_m = 1.23d = 2.50$ Å. This value agrees with the determination of Hampel *et al.,* [14], who found $x_m = 2.5$ Å. A bright field micrograph of a sample irradiated up to a fluence of 1×10^{11} ions $\cdot$ cm^{-2} is shown in Fig. 1(b). White spots corresponding to the impacts of the projectiles are clearly visible. The density of these spots, corresponding to the ion fluence, indicates that each projectile locally induces damage which is visible by TEM. The observed diameters of the damage range from 6.8 to 7.5 nm. The corresponding electron diffraction pattern [Fig. 1(d)] shows clear differences from the initial one [Fig. 1(c)]. The diffraction rings are named, respectively, A and C for amorphous and crystalline contributions and have increasing numbers as the radii on the diffraction pattern increase. There are two diffuse rings ($A1$ and $A2$) characteristic of the amorphous structure and, in addition, four thin continuous rings (hereafter named $C1$ to $C4$) characteristic of crystalline matter. Two of them ($C1$ and $C2$) correspond to radii smaller than that of the first amorphous ring $A1$; the two others ($C3$ and $C4$) are located between rings $A1$ and $A2$. Figure 2(a) presents an HRTEM micrograph of an isolated damage region from a 5 GeV Pb ion. The experimental image was taken at the Scherzer defocus ($D_f = -90$ nm). We observe that the track diameter is 6–8 nm and that the track core is amorphous. Nanocrystallites, with a size ranging between 1 and 4 nm, are observed around the ion track.

TABLE I. Ion fluence, diameter of the damaged regions, observed diffraction rings, associated interplanar distances, and most probable phases in the irradiated sample.

Fluence (cm^{-2})	Diameter (nm)	Diffraction rings	Average interplanar distance (Å)	Possible phase
0		$A1$	2.03(3)	Amorphous
		$A2$	1.20(7)	$x_m = 2.50$ Å
10^{11}	6.8–7.5	$A1, A2$		Amorphous
		$C1$	2.56(1)	Fe_2B
		$C2$	2.43(5)	$Fe_{23}B_6$
		$C3$	1.59(4)	$Fe_{23}B_6$
		$C4$	1.48(0)	$Fe_{23}B_6$

A corresponding Fourier transform (FT) plot shows the presence of diffraction spots characteristic of Fe_2B and $Fe_{23}B_6$ crystalline structures [Fig. 2(b)]. These spots correspond, respectively, to the $C1$ and $C2$ crystalline rings in Fig. 1(d). In Fig. 2(b) we observe only a few diffraction spots, whereas almost continuous dotted diffraction rings are seen in Fig. 1(d); this is due to the fact that a very local information is obtained from FT analysis, in which only a few crystallites contribute to the FT image.

Discussion and conclusion.—The average interplanar distances corresponding to the crystalline rings that were found on the electron diffraction patterns of the irradiated samples have been compared to the calculated interplanar distances of the main crystalline phases that appear during annealing of the $Fe_{73.5}Cu_1Nb_3Si_{13.5}B_9$ alloy. In the last column of Table I we report the most probable phases that could correspond to the TEM results. We emphasize that this identification shows that the observed distances agree reasonably well with the interplanar distances of face centered cubic $Fe_{23}B_6$ (and for one line with those of tetragonal Fe_2B). However, since some strains could exist in the nanocrystals that form, this could lead to significant deviations of the interplanar distances from the thermal equilibrium ones. We did not observe any evidence of the formation of the Fe(Si) phase.

Which process could induce the crystallization?—Because amorphous alloys do not exist in thermodynamic equilibrium, they can undergo crystallization if energy is supplied. The crystallization of $Fe_{73.5}Cu_1Nb_3Si_{13.5}B_9$ by annealing takes place in two steps: when the annealing temperature exceeds about 520 °C, a partial crystallization occurs and results in the formation of a nanostructure which consists of nanograins of bcc Fe(Si) [12] with a well defined grain size ($\sim$ 10 nm) embedded in a residual amorphous matrix. Such a nanocrystalline alloy (named FINEMET) reveals excellent soft magnetic properties. The increase of the annealing temperature above about 670 °C causes a complete crystallization of the amorphous matrix and the formation of iron borate compounds

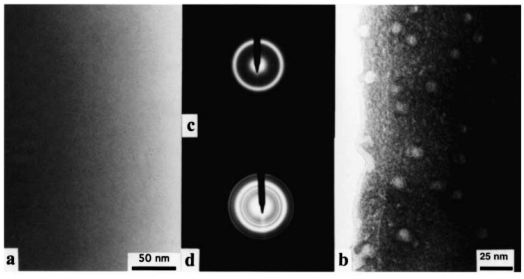

FIG. 1. TEM (a) and corresponding electron diffraction pattern (c) of an unirradiated $Fe_{73.5}Cu_1Nb_3Si_{13.5}B_9$ amorphous sample. Bright field TEM micrograph (b) of a $Fe_{73.5}Cu_1Nb_3Si_{13.5}B_9$ amorphous sample irradiated at normal incidence and below 90 K with 5 GeV Pb ions with a fluence of 1×10^{11} ions $\cdot$ cm^{-2}. The corresponding electron diffraction pattern is given in (d).

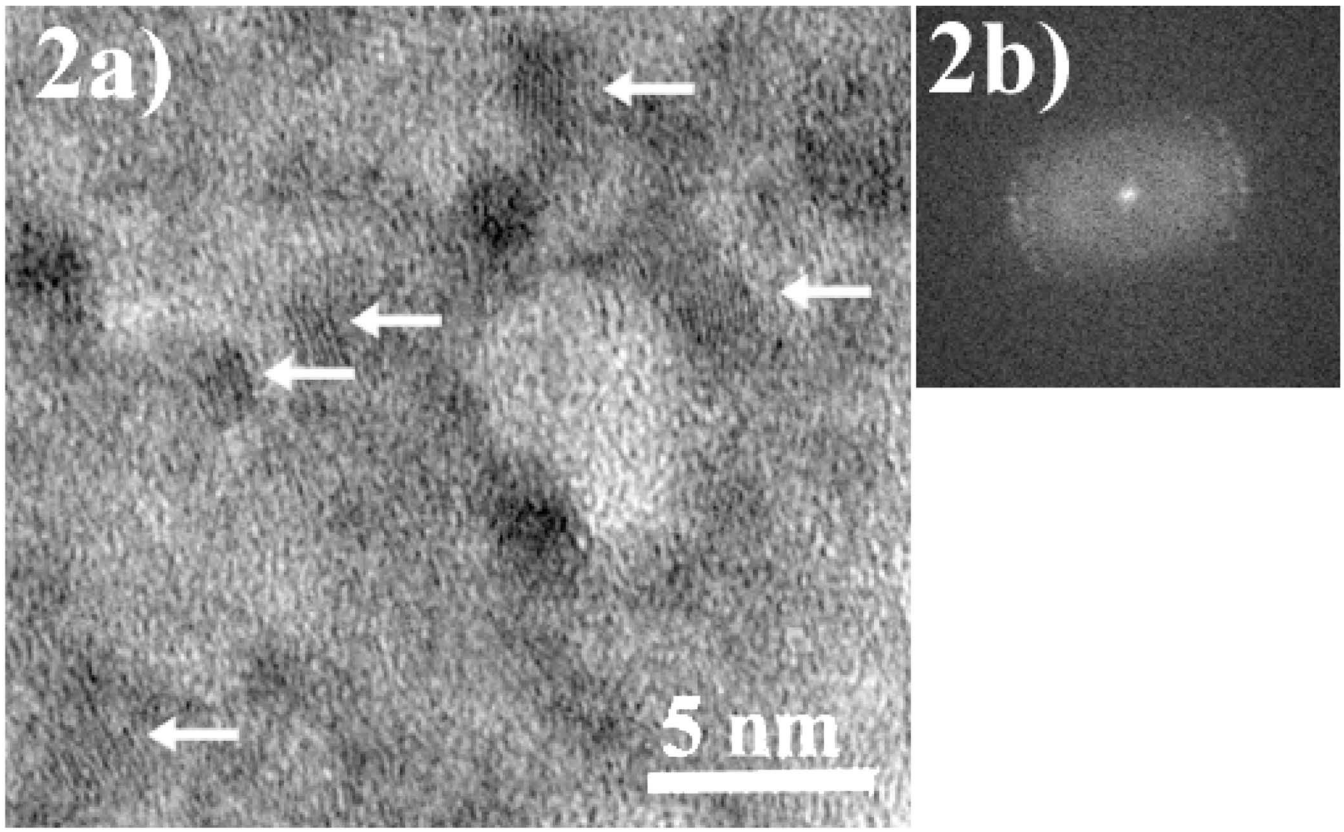

FIG. 2. HRTEM image of an ion track in an $Fe_{73.5}Cu_1Nb_3Si_{13.5}B_9$ amorphous sample irradiated with 5 GeV Pb ions to a fluence of 1×10^{11} ions $\cdot$ cm^{-2} (a). We observe that (i) the track core remains amorphous and (ii) nanocrystallites (indicated by the arrows), with 1–4 nm diameter, appear in the vicinity of the ion track. The presence of crystalline nanostructures is confirmed by the diffraction spots in the corresponding Fourier transform plot (b).

(Fe_2B, Fe_3B, $Fe_{23}B_6$, ...) [12,15–17]. When the size of the crystalline grains grows, the soft magnetic properties dramatically deteriorate.

In addition to the annealing-induced crystallization, recently, processes of crystallization of amorphous alloys driven by mechanical milling [18] and nanoindentation [19] have been reported. Previous research has shown that mechanical crystallization is different from thermal crystallization and cannot be attributed only to a local effective temperature, but may be related to a change of the nucleation barrier with the chemical composition of the amorphous alloys [18–22].

Energy conversion into atomic movement.—During the slowing down of GeV heavy projectiles, the energy lost by the particle is mainly transmitted to the target through electronic excitation processes. This energy is primarily deposited in the close vicinity of the projectile path. Two different models were often proposed to account for damage creation: the thermal spike model and the Coulomb explosion model. In the thermal spike model the relaxation of the excess of energy may occur via energy transfers from the excited electronic system to target atoms and can lead to a local "temperature" increase [23,24]. This temperature increase is not easy to define and to evaluate quantitatively since energy deposition is a non-equilibrium phenomenon and can lead to contradictory estimates in the literature [24–27]. Nevertheless, as we mainly observe the formation of the crystalline phases which are formed in the second crystallization step, we could infer that, following the assumption of the "thermal spike" approach, the "local temperature" in the track region reached values well above 670 °C for a sufficiently long time so that crystallization of iron borates can take place.

In the Coulomb repulsion model the relaxation of the localized excess of energy occurs via radial impulses of atoms lying in the vicinity of the ion path [28–30]. The atomic movements consist of a collective and coherent repulsion of atoms (shock wave) without a significant increase of the local temperature. In both models, the relaxation of the excess of energy is followed by a time-dependent acoustic wave within about 10^{-15} s. The generation of a radial shock wave or of a "pressure pulse" [30,31] may favor damage creation because, due to this radial impulse, stress and strain is created around each ion track [32] and can expand radially to fairly large distances. This may explain that in Fig. 2(a), nanocrystals are formed even as far as 15 nm from the ion path. It is well known that the presence of strain or excess of free volume in amorphous alloys may reduce the activation

energy for atomic rearrangement associated with structural relaxation [20,21]. We conclude that irradiation-induced stress and strain might destabilize the amorphous structure at temperatures below crystallization temperature and induce the observed nanocrystallization of the target.

We finally want to indicate that irradiation-induced crystallization may just concern amorphous alloys that crystallize in two steps. In fact, after irradiation of a "conventional" amorphous alloy ($Fe_{40}Ni_{35}Si_{10}B_{15}$) with Pb ions using the GANIL accelerator, no sign of crystallization was detected by TEM after irradiation at fluences of 1×10^{11} and 1×10^{12} ions $\cdot$ cm^{-2}. It was found that this alloy follows the usual behavior, so that only surface deformations could be seen by TEM [33]. These two types of amorphous alloys have similar melting temperatures, thermal conductivities, and crystallization temperatures ($\sim 520\,^{\circ}$C) [16,17,34]. The only relevant difference is that an amorphous $Fe_{40}Ni_{35}Si_{10}B_{15}$ alloy crystallizes in one step. The different crystallization behaviors of these two types of amorphous alloys could also be related to the presence of copper atoms which act as nucleation centers in the crystallization process.

In conclusion, we have demonstrated that low temperature irradiation of an amorphous $Fe_{73.5}Cu_1Nb_3Si_{13.5}B_9$ alloy with 5 GeV Pb ions induces local crystallization in the amorphous phase, which was not seen in experiments performed with other amorphous alloys. The TEM analysis indicates that iron borides are formed. No evidence for the formation of the Fe(Si) phase was found. The observed crystallization results from the local relaxation of the energy deposited in the target electronic system along the ion trajectory and is not due to the bulk heating of the sample by the ion beam which we can definitively exclude.

The authors thank all the staff of the CIRIL laboratory for their help during the irradiation and, in particular, J. M. Ramillon for his very efficient technical assistance.

*Electronic address: annie.dunlop@polytechnique.fr

[1] S. Klaumünzer, G. Schumacher, S. Rentzsch, G. Vogl, L. Soldner, and H. Bieger, Acta Metall. **30**, 1493 (1982).
[2] A. Audouard, E. Balanzat, G. Fuchs, J.C. Jousset, D. Lesueur, and L. Thomé, Europhys. Lett. **3**, 327 (1987); Nucl. Instrum. Methods Phys. Res., Sect. B **39**, 18 (1989).
[3] S. Klaumünzer, Changlin Li, S. Loffler, M. Rammensee, G. Schumacher, and H. Ch. Neitzert, Radiat. Eff. Defects Solids **108**, 131 (1989).
[4] A. Audouard, M. Toulemonde, G. Szenes, and L. Thomé, Nucl. Instrum. Methods Phys. Res., Sect. B **146**, 233 (1998).
[5] Ming Dong Hou, S. Klaumünzer, and G. Schumacher, Phys. Rev. B **41**, 1144 (1990).
[6] A. Audouard, E. Balanzat, J.C. Jousset, D. Lesueur, and L. Thomé, J. Phys. Condens. Matter **5**, 995 (1993).
[7] A. Barbu, A. Dunlop, and D. Lesueur, Europhys. Lett. **15**, 37 (1991).
[8] A. Iwase, S. Sasaki, T. Iwata, and T. Nihira, Phys. Rev. Lett. **58**, 2450 (1987).
[9] A. Dunlop, D. Lesueur, P. Legrand, H. Dammak, and J. Dural, Nucl. Instrum. Methods Phys. Res., Sect. B **90**, 330 (1994).
[10] A. Dunlop, G. Jaskierowicz, and S. Della Negra, C. R. Acad. Sci., Ser. IIb: Mec., Phys., Chim., Astron. **325**, 397 (1997).
[11] A. Dunlop, J. Henry, and G. Jaskierowicz, Nucl. Instrum. Methods Phys. Res., Sect. B **146**, 222 (1998).
[12] Y. Yoshizawa, S. Oguma, and K. Yamauchi, J. Appl. Phys. **64**, 6044 (1988).
[13] A. Guinier, *Théorie et Technique de la Radiocristallographie* (Dunod, Paris, 1964), p. 452.
[14] G. Hampel, A. Pundt, and J. Hesse, J. Phys. Condens. Matter **4**, 3195 (1992).
[15] P. Gorria, J.S. Garitaonandia, and J.M. Barandiaran, J. Phys. Condens. Matter **8**, 5925 (1996).
[16] N. Kataoka, A. Inoue, T. Masumoto, Y. Yoshizawa, and K. Yamauchi, Jpn. J. Appl. Phys. **28**, 1820 (1989).
[17] T. Kulik and A. Hernando, Mater. Sci. Forum **179–181**, 587 (1995).
[18] M. L. Trudeau, R. Schulz, D. Dussault, and A. Van Neste, Phys. Rev. Lett. **64**, 99 (1990).
[19] J.J. Kim, Y. Choi, S. Suresh, and A.S. Argon, Science **295**, 654 (2002).
[20] F. Spaepen, Acta Metall. **25**, 407 (1977).
[21] A.S. Argon, Acta Metall. **27**, 47 (1979).
[22] H. Chen, Y. He, G.J. Shiflet, and S.J. Poon, Nature (London) **367**, 541 (1994).
[23] L.T. Chadderton and H.M. Montagu-Pollok, Proc. R. Soc. London A **274**, 239 (1969).
[24] M. Toulemonde, C. Dufour, and E. Paumier, Phys. Rev. B **46**, 14362 (1992).
[25] Yu. V. Martynenko and Yu. N. Yavlinskii, Sov. Phys. Dokl. **28**, 391 (1983).
[26] A. Miotello and R. Kelly, Nucl. Instrum. Methods Phys. Res., Sect. B **122**, 458 (1997).
[27] A. Volkov and V.A. Borodin, Nucl. Instrum. Methods Phys. Res., Sect. B **146**, 137 (1998).
[28] R.L. Fleischer, P.B. Price, and R.M. Walker, J. Appl. Phys. **36**, 3645 (1965).
[29] I.S. Bitensky and E.S. Parilis, Nucl. Instrum. Methods Phys. Res., Sect. B **21**, 26 (1987).
[30] D. Lesueur and A. Dunlop, Radiat. Eff. Defects Solids **126**, 163 (1993).
[31] R.E. Johnson, B.U.R. Sundqvist, A. Hedin, and D. Fenyö, Phys. Rev. B **40**, 49 (1989).
[32] H. Trinkaus, Nucl. Instrum. Methods Phys. Res., Sect. B **107**, 155 (1996).
[33] A. Dunlop *et al.* (to be published).
[34] M. Kopcewicz, E. Jackiewicz, L. Zaluski, and A. Zaluska, J. Appl. Phys. **71**, 3997 (1992).